EFFICIENT APPROACH FOR MULTIPOINT AERODYNAMIC WING DESIGN OF BUSINESS JET AIRCRAFT

Sergey Peigin, Boris Epstein
Israel Aerospace Industries, The Academic College of Tel-Aviv Yaffo

Keywords: *Constarined optimization, Genetic Algorithm, Navier-Stokes driver, parallel computations*

Abstract

An efficient CFD driven approach to multipoint constrained aerodynamic wing design for business jet aircraft is proposed. In the framework of the method, the total drag of an optimized aircraft configuration is minimized at fixed lift values subject to numerous geometrical and aerodynamical constraints. The optimum search is driven by Genetic Algorithms and is based on full Navier-Stokes computations supported by massive multilevel parallelization. The applications include a series of single- and multi-point aerodynamic design optimizations for a generic business jet. For the considered class of shape optimizations, significant drag reduction in on- and off-design conditions has been achieved.

1 Introduction

The growing competitiveness in aircraft industry calls for accurate, efficient and robust tool for advanced aerodynamic shape design. The main goal of such a tool is to produce a configuration suited to the aircraft mission with as low as possible flight costs.

In the development of commercial aircraft, aerodynamic design plays a leading role during the preliminary design stage where the external aerodynamic shape is typically finalized. This phase is estimated by a cost of 60-120 million dollars [1]. The final design would be normally carried out only upon the commercially promising completion of the preliminary stage which makes the preliminary design stage crucial for the overall success of the project.

The aerodynamic design process is embedded in the overall preliminary design with the starting point coming from the conceptual design. The inner loop of aerodynamic analysis is included into an outer (multidisciplinary) loop which is a part of a major design cycle. Due to the limitations of the overall design technology, this cycle is usually repeated a number of times. Thus the introduction of a CFD driven robust automatic aerodynamic optimization, which will allow to reduce the number of design cycles, would significantly shorten the overall design process.

The past three decades brought a revolution in the entire process of aerodynamic design due to the increasing role of computational simulation.

In the beginning, the applicability of CFD to the aerodynamic design was confined to flow analysis in a limited range of flight conditions and aerodynamic shapes. Additional limitations were due to the variable accuracy level in prediction of different aerodynamic characteristics.

Over the years CFD driven optimization methods appeared [1]-[9]. Though the subject has aroused considerable interest in many researchers and aircraft companies, the practical impact of available optimization techniques is, to the best of our knowledge, rather limited from the industrial viewpoint.

In this context, the main goal of this paper is to present an accurate and computationally efficient approach to the multipoint constrained aerodynamic design for business jet aircrafts. In the framework of the method, the total drag of an optimized aircraft configuration is minimized

at fixed lift values subject to numerous geometrical and aerodynamical constraints. The optimum search is driven by Genetic Algorithms and is based on full Navier-Stokes drag prediction, supported by massive multilevel parallelization of the whole computational framework.

The applications include a series of single- and multi-point aerodynamic optimizations for a generic business jet. It was demonstrated that the proposed method allows to design feasible aerodynamic shapes which possess a low drag at cruise conditions, satisfy a large number of geometrical and aerodynamic constraints and offer a good off-design performance in markedly different flight conditions such as take-off and high Mach zone.

2 Statement of the Problem

The input parameters of the aerodynamic configuration design include prescribed cruise lift, Mach, altitude and minimum allowed drag values which should ensure the aerodynamic goals of the aircraft mission (such as range, payload, fuel volume etc). The desired geometry is sought in the class of solutions which satisfy different geometrical, aerodynamic and multidisciplinary constraints.

The design goal is to develop a geometry with as low a drag at cruise conditions as possible which, at the same time, satisfies the above constraints.

The main idea behind the proposed approach is to accomplish this objective through a CFD-based solution of the properly formulated multipoint constrained optimization problem.

The set of constraints may be divided into the following two classes: the class of geometrical constraints and the class of aerodynamic constraints. The geometrical constraints are mostly independent of flight conditions and are easily verified while aerodynamic constraints naturally depend on flight conditions, and necessitate heavy CFD runs for their verification.

Concerning the choice of the objective function, it is assumed that the drag coefficient C_D of a tested configuration is a sensitive and reliable indicator of its aerodynamic performance and thus we employ C_D as the objective function of the considered optimization problem.

Another crucial issue is the implementation of constraints in the framework of the optimization algorithm. Where possible, the constraints should be satisfied exactly in the direct way while the remaining constraints should be converted into alternative constraints which can be expressed in terms of drag. For example, in the proposed approach the geometrical constraints and such aerodynamic constraints as the prescribed lift coefficient are satisfied exactly while the requirement of a sufficiently high C_L^{max} at the take-off conditions is reformulated in terms of drag at the corresponding flight conditions.

Finally in order to ensure the accuracy of optimization we require that for any geometry feasible from the constraints' viewpoint, the value of the objective (cost) function remains exactly equal to the value of the drag coefficient without any penalization.

Based on the above ideas, the mathematical formulation of the optimization problem whose solution allows to achieve the design goal may be expressed as follows.

The objective of the general multipoint optimization problem is to minimize the weighted combination C_D^{wtd} of drag coefficients at the main design and secondary design points (flight conditions)

$$C_D^{wtd} = \sum_{k=1}^{K} w_k C_D(k)$$

where K is the total number of the design points.

The solution is sought in the class of wing shapes subject to the following classes of constraints:

1) Aerodynamic constraints such as prescribed constant total lift coefficient $C_L^*(k)$ and maximum allowed pitching moment $C_M^*(k)$:

$$C_L(k) = C_L^*(k), \quad C_M(k) \geq C_M^*(k) \qquad (1)$$

2) Geometrical constraints on the shape of the wing surface in terms of properties of sectional airfoils at the prescribed wing span locations: relative thickness $(t/c)_i$, relative local

thickness $(\Delta y/c)_{ij}$ at the given chord locations $(x/c)_{ij}$ (beam constraints), relative radius of leading edge $(R/c)_i$, trailing edge angle θ_i:

$$(t/c)_i \geq (t/c)_i^*, \quad (\Delta y/c)_{ij} \geq (\Delta y/c)_{ij}^*, \qquad (2)$$

$$(R/c)_i \geq (R/c)_i^*, \quad \theta_i \geq \theta_i^*$$

$$i = 1,\ldots,N_{ws}, \quad j = 1,\ldots,N_{bc}(i)$$

where N_{ws} is the total number of sectional airfoils subject to optimization, $N_{bc}(i)$ is the total number of beams constraints at section i, and values $(t/c)_i^*$, $(\Delta y/c)_{ij}^*$, θ_i^*, $(R/c)_i^*$, C_L^* and C_M^* are prescribed parameters of the problem.

Thus in the present work the total number of considered constraints N_{cs} is equal to

$$N_{cs} = 2 \times K + 3 \times N_{ws} + \sum_{i=1}^{N_{ws}} N_{bc}(i)$$

In principle, the present optimization method allows for handling a large number of constraints of different nature in addition to the above described ones.

As a gas-dynamic model for calculating C_D, C_L and C_M values, the full Navier-Stokes equations are used. Numerical solution of the full Navier-Stokes equations was provided by the multiblock code NES [11] which employs structured point-to-point matched grids. The code is based on the Essentially Non-Oscillatory (ENO) concept with a flux interpolation technique which allows for accurate estimation of sensitive aerodynamic characteristics such as lift, pressure drag, friction drag and pitching moment.

The code ensures high accuracy of the Navier-Stokes computations and high robustness for a wide range of flows and geometrical configurations. The important advantage of the solver NES as a driver of optimization process is its ability to provide reliable and sufficiently accurate results already on relatively coarse meshes and thus to reduce dramatically the volume of CFD computations.

3 Optimization Algorithm

In this section, we briefly describe the optimization method recently developed by the authors. Two-dimensional applications of the method may be found in [13], while the optimization of isolated 3D wings was considered in [10].

The driver of the optimization search is a variant of Genetic Algorithms (GAs). The main features of the method include a new strategy for efficient handling of nonlinear constraints in the framework of GAs, scanning of the optimization search space by a combination of full Navier-Stokes computations with the Reduced Order Models (ROM) method and multilevel parallelization of the whole computational framework which efficiently makes use of computational power supplied by massively parallel processors (MPP).

3.1 Search Space Parameterization

An optimization process can be described as a path in the search space, the points of which represent different geometries. Thus the choice of an appropriate search space is of crucial importance.

In practice, the initial geometry of the configuration comes in the form of a CAD representation or already as a 3D numerical grid (needed for CFD estimation of the objective function). Note, that in the former case, the CAD files should be converted into a CFD grid. In both cases, an aerodynamic surface is represented by a set of local patches, and each patch is a set of discrete points. The total number of surface points may amount to 100 000.

The search space should include a sufficiently wide spectrum of geometrical shapes. The local shape description above satisfies this requirement but results in very high dimensions of the search space. On the other hand, since the complexity of optimal search grows exponentially with the search space dimensions, the total number of parameters should not be too high (in order to ensure a successful and efficient search).

Hence, a global representation of aerodynamic surfaces is needed. The main requirements

for such a representation are the following. It should be based on a limited number of parameters, should ensure a sufficient shape representativeness and additionally, points close one to each other in the search space should yield close CFD grids.

In the following, it is assumed that the geometry of the aircraft configuration is described in the absolute Cartesian coordinate system (x,y,z), where the axes x, y and z are directed along the streamwise, normal to wing surface and span directions, respectively. In the developed approach, the whole surface of a wing body configuration is divided into three parts. The first part contains the points of the aircraft fuselage "inboard of the fairing". This part of the configuration is not subject to modification.

The second part contains the points of the exposed wing "outboard of the fairing". This part of the configuration is represented by a linear interpolation of 2D cuts (wing sections), For each wing section, the non-dimensional shape of the airfoil (scaled by the corresponding chord) is defined in a local Cartesian coordinate system $(\bar{x},\bar{y})$ in the following way. The coordinates of the leading edge and trailing edge of the profile were respectively $(0,0)$ and $(1,0)$. For approximation of the upper and lower airfoil surface, Bezier curve (one-dimensional Bezier Spline) representation was used. A Bezier curve of order N is defined by the Bernstein polynomials $B_{N,i}$ (C_N^i - binomial coefficients)

$$\vec{G}^k(t) = \sum_{i=0}^{N} B_{N,i}\vec{P}_i^k, \qquad (3)$$

$$B_{N,i} = C_N^i t^i (1-t)^{N-i}, \quad C_N^i = \frac{N!}{i!(N-i)!},$$

where t denotes the curve parameter taking values in $[0,1]$, $\vec{P}_i^k$ are the control points and superscript $k = u,l$ corresponds to upper and lower surfaces of profile. So, as it is seen from (3), the Bezier curve is completely determined by the Cartesian coordinates of the control points. Additional parameters of optimization are twist angles $\{\alpha_i^{tw}\}$ and dihedral values $\{\gamma_i^{dh}\}$.

Finally, the third (highly non-linear) part of the configuration is the fairing. This essentially 3D part is described through combination of Bezier surfaces representation (two-parameter families of Bezier Splines) and local twist distribution (one-parameter Bezier Spline).

3.2 Search Algorithm

As a basic search algorithm, a variant of the floating-point GA [14] is used. The mating pool is formed through the use of tournament selection. This allows for an essential increase in the diversity of the parents. We employ the arithmetical crossover and the non-uniform real-coded mutation defined by Michalewicz [14]. To avoid a premature convergence of GA we applied the mutation operator in a distance-dependent form. To improve the convergence of the algorithm we also use the elitism principle.

In the considered optimization problem, the presence of constraints has a great impact on the solution. This is due to the fact that the optimal solution does not represent a local minimum in the conventional sense of the word. Instead, it is located on an intersection of hypersurfaces of different dimensions, generated by linear and nonlinear constraints. Additionally, the problem of finding such an extremum is essentially complicated by the fact that these hypersurfaces, which bound the feasible search space, are not known in advance and may possess irregular topology.

For example, it is aerodynamically expected that in the case of the thickness-constrained optimization, the optimal wing should possess the minimum allowed thickness. This implies that the optimal point should reside exactly on the corresponding hypersurface.

In the case of constraints, imposed on the aerodynamic characteristics such as pitching moment C_M, the situation is even less controlled. Similar to the previous example, the optimal solution should be located exactly on the constraint boundary. But contrary to the case of geometrical constraints, the determination of the boundary is a much heavier computational problem. For the geometrical constraints, the feasibility test is

computationally very cheap while in the case of aerodynamic constraints, the corresponding test requires a full (computationally heavy) CFD run.

In their basic form, Genetic Algorithms are not capable of handling constraint functions limiting the set of feasible solutions. To resolve this, a new approach has been proposed which can be basically outlined as follows:

A) Instead of the traditional approach where only feasible points may be included in a path, it is proposed to employ search paths through both feasible and infeasible points

B) With this end in view, the search space is extended by evaluating (in terms of fitness) the points, which do not satisfy the constraints imposed by the optimization problem. A needed extension of an objective function may be implemented by means of GAs due to their basic property: contrary to classical optimization methods, GAs are not confined to only smooth extensions.

3.3 Approximation of Objective Function

Low computational efficiency of GAs is the main obstacle to their practical use where the evaluation of the cost function is computationally expensive as it happens in the framework of the full Navier-Stokes model.

A simple estimation demonstrates that even for a moderate population size of $\mathbf{M}$= 100 at least 20000 evaluations of the cost function (CFD solutions) are required to reach the appropriate convergence. A fast full Navier-Stokes evaluation over a 3D wing-body aircraft configuration takes at least a 30-40 minutes of CPU time. Consequently, the direct use of such an algorithm is practically unacceptable.

To resolve this problem, we employ an intermediate “computational agent” - a computational tool which, on the one hand, is based on a very limited number of exact evaluations of objective function and, on the other hand, provides a fast and reasonably accurate computational feedback in the framework of GAs search.

In this work we use Reduced-Order Models approach, where the solution functionals are approximated by a local data base. The data base is obtained by solving the full Navier-Stokes equations in a discrete neighbourhood of a basic point (basic geometry) positioned in the search space. Specifically a mixed linear-quadratic approximation is employed. One-dimensionally, the one-sided linear approximation is used in the case of monotonic behaviour of the approximated function, and the quadratic approximation is used otherwise.

In order to ensure the accuracy and robustness of the method a multidomain prediction-verification principle is employed. That is, on the prediction stage the genetic optimum search is concurrently performed on a number of embedded search domains. As the result each domain produces an optimal point, and the whole set of these points is verified (through full Navier-Stokes computations) on the verification stage of the method, and thus the final optimal point is determined. It is important to note that actually, the Navier-Stokes computations are performed only for the data-base construction ($2N_D$ computations) and for the verification of optimal points (the number of computations is equal to the number of search domains). More details can be found in Ref. [13].

Besides, in order to ensure the global character of the search, it is necessary to overcome the local nature of the above approximation. For this purpose it is suggested to perform iterations in such a way that in each iteration, the result of optimization serves as the initial point for the next iteration step (further referred to as optimization step).

3.4 Parallelization of the Optimization Stream

The problem of optimization of aerodynamic shapes is very time-consuming as it requires a huge amount of computational work. Each optimization step requires a number of heavy CFD runs, and a large number of such steps is needed to reach an optimum. Thus the construction of a computationally efficient algorithm is vital for the success of the method in engineering environment.

To reach this goal it was proposed to employ an embedded multilevel parallelization strategy which includes: Level 1 - Parallelization of full Navier-Stokes solver; Level 2 - Parallel CFD scanning of the search space; Level 3 - Parallelization of the GAs optimization process; Level 4 - Parallel optimal search on multiple search domains and Level 5 - Parallel grid generation.

The first parallelization level (for a detailed description see [15]) is based on the geometrical decomposition principle. All processors are divided into two groups: one master-processor and N_s slave-processors. A large body of computational data demonstrated that the above approach for parallel implementation of the multiblock full Navier-Stokes solver, enables one to achieve high level of parallel efficiency while retaining high accuracy of calculations, and thus to significantly reduce the execution time for large-scale CFD computations.

The first level of parallelization is embedded with the second level, which performs parallel scanning of the search space and thus provides parallel CFD estimation of fitness function on multiple geometries.

The third level parallelizes the GAs optimization work unit. At this level of parallelization, all the processors are divided into one master-processor and P_s slave-processors. The goal of the master-processor is to distribute the initial random populations among the slaves and to get back the results of optimal search (P_s is the number of initial random populations).

The third level of parallelization is embedded with the fourth level, which performs parallel optimal search on multiple search domains. At this level of parallelization all the processors are divided into three groups: one main-processor, P_m master-processors and $P_m \cdot P_s$ of slave-processors (where P_m is equal to the number of domains).

The fifth parallelization level handles the grid generation process. At this level, one master-processor and G_s slave-processors are employed (G_s is the number of evaluated geometries).

Finally we can conclude that the five-level parallelization approach allowed us to sustain a high level of parallel efficiency on massively parallel machines, and thus to dramatically improve the computational efficiency of the optimization algorithm.

4 Analysis of Results

The method was applied to the problem of multi-point multiconstrained transonic wing optimization for a generic business jet aircraft. The configuration includes a realistic fuselage, wing-body fillet and a cranked glove-like high aspect-ratio wing.

The CFD solver NES (used as a driver of the optimization process) ensures high accuracy of the Navier-Stokes computations on relatively coarse grids as well as high robustness, for a wide range of flows and geometrical configurations. High performance of NES was systematically demonstrated by testing it a wide range of aerodynamic configurations of different complexity: from one-element 2D airfoils through transport-type supercritical wings up to full wing-body configurations [11],[12],[16]. The results by the code NES demonstrated a high accuracy of drag prediction (within several counts) in the whole range of flight conditions. Note, that the prediction accuracy of component drag increments (with nacelle on and off) was even higher. This is indicative of the NES suitability as a CFD driver of optimization process.

For transonic wing-body configurations, NES provides accurate asymptotically converged estimates of aerodynamic coefficients with C-O topology grids containing on the fine level about 325 points around the configuration, 57 points normal to the surface and 49 points in the spanwise direction.

In the following, we present the results of one- and multi-point drag minimization for a generic business jet aircraft. The geometrical constraints (per section) were placed upon relative maximum thickness, local relative leading edge radius (the radius of curvature of a non-dimensional wing section at $\bar{x} = 0$) and trailing edge angle as well as relative local thickness at two fixed x/c locations (beam constraints). An additional (aerodynamic) constraint was imposed

Case No.	C_L^*	M	C_M^*	$N_{bc}(i)$
Case_GBJ_1	0.52	0.75	$-\infty$	0
Case_GBJ_2	0.40	0.80	$-\infty$	0
Case_GBJ_3	0.40	0.80	$-\infty$	2
Case_GBJ_4	0.40	0.80	-0.136	0
Case_GBJ_5	0.40	0.80	-0.136	2
Case_GBJ_6	0.40	0.80	-0.136	2
	1.50	0.20	$-\infty$	2
Case_GBJ_7	0.40	0.80	-0.136	2
	1.50	0.20	$-\infty$	2
	0.40	0.82	-0.150	2

Table 1 Generic business jet wing-body configuration. Wing optimization conditions and constraints.

on the value of pitching moment. In all the considered test-cases, the values of all the above geometrical constraints were kept to the level of the original geometry.

The design conditions and constraints are summarized in Table 1. The corresponding optimal shapes are designated by *Case_GBJ_*1 to *Case_GBJ_*7.

The first 5 cases deal with one-point optimization at two design points: $C_L = 0.52$, $M = 0.75$ and $C_L = 0.40$, $M = 0.80$ with different constraints placed upon the solution. The last 2 cases are related to multi-point optimization.

The original generic wing-body configuration possesses a moderate shock at $C_L = 0.52$, $M = 0.75$. The shock covers most of the wing span being especially strong in the vicinity of crank. In terms of drag the shock leads to a relatively high total drag value of the initial configuration - $C_D = 317.5$ aerodynamic counts.

The performed one-point optimization allowed to essentially reduce the drag. Specifically, with no constraint placed upon the pitching moment (*Case_GBJ_*1), the total drag amounts to 304.1 counts. Though the maximum thickness of wing sections remained unchanged, the wing loading for the optimal geometry was strongly redistributed compared to the original one and the resulted pressure distribution is virtually shockless.

The drag reduction due to optimization is not pointwise. In terms of lift/drag curves this gain is preserved in a wide range of C_L values. Moreover, the drag reduction is only higher at higher lift coefficients.

The second considered design point possesses a higher free-stream Mach number and a lower C_L value: $M = 0.80$, $C_L = 0.40$. This combination of flight conditions leads to a significant change in the shock pattern. In particular, as it can be assessed from the corresponding pressure distributions in Fig. 1-2, the original configuration is characterized by a λ -like spanwise shock development. At these conditions the original configuration drag value is equal to $C_D = 292.0$ aerodynamic counts.

The performed unconstrained (with respect to C_M) one-point optimizations (*Case_GBJ_*2 and *Case_GBJ_*3) allowed to reduce the drag to 275.3 and 275.9 counts, respectively. As it is seen from Table 1, in *Case_GBJ_*3 an additional constraint (compared to *Case_GBJ_*2) was imposed on local wing thickness at specified points (beam constraints).

The corresponding pressure distributions are depicted in Fig.3 - 4. The analysis of these pictures allowed to conclude that the achieved drag reduction may be attributed to a significant decrease in the shock strength.

Off-design behaviour of optimized configurations may be studied through lift/drag polars. These are presented in Fig.5, where the corresponding curves at $M = 0.80$ are compared with the original polar thus illustrating the influence of the beam constraints on the results of optimization.

It can be concluded that the above described local gains are preserved in a wide range of lift coefficient values from $C_L = 0.15$ to above $C_L = 0.6$. Additionally we should note that the two optimized curves are close one to another especially in a large vicinity of the design C_L. At the same time, in terms of shape, the difference between these optimization cases is significant for the both crank and tip wing sections (see Fig.6).

Alongside the unconstrained pitching mo-

ment optimizations, the optimizations with constraint on C_M^*, were performed. In *Case_GBJ_*4 and *Case_GBJ_*5 the value of C_M^* was kept to the original level (C_M^* = -0.136). These two cases differ in the presence of beam constraints, which were only imposed in *Case_GBJ_*5.

Let us compare the optimizations of *Case_GBJ_*2-*Case_GBJ_*3 vs. *Case_GBJ_*4-*Case_GBJ_*5. As a whole, the penalty due to the imposition of pitching moment constraint was practically negligible: C_D=275.7 counts for *Case_GBJ_*4 (about 0.4 counts higher with respect to *Case_GBJ_*2) and C_D=276.1 counts for *Case_GBJ_*5 (0.2 counts higher compared to *Case_GBJ_*3).

The comparison of the corresponding pressure distributions (Fig.3 vs. Fig.7) shows that the inclusion of the above constraint resulted (as aerodynamically expected) in a higher loading of the leading edge area of the wing, especially of its inboard part.

In terms of shape modification, the influence of the optimization parameters on the specific form of the wing tip section can be assessed from Fig.8. It is interesting, that the optimization algorithm (operating in the automatic mode) employs very different ways to achieve its goals for different sets of constraints (especially in the wing leading edge region). Specifically, for *Case_GBJ_*4 a solution with the significant leading edge droop was found, while for *Case_GBJ_*5 the droop is only weakly indicated and the wing possesses a higher volume.

From the both theoretical and practical view points it is interesting to know whether the optimal shapes are unique. The above comparison of optimal shapes provides a clarifying example on the subject. We see that very close values of total drag may correspond to significantly different wing geometries.

The last two cases (*Case_GBJ_*6-*Case_GBJ_*7) are related to two- and three-point optimizations which take into account the full set of constraints. In *Case_GBJ_*6 cruise and take-off conditions were targeted, while in *Case_GBJ_*7 the additional design point at a higher $M = 0.82$ was added.

The results were as follows. At the main design point ($C_L = 0.40$ $M = 0.80$) the total drag value for *Case_GBJ_*6 was equal to 276.1 counts compared to 275.6 counts for *Case_GBJ_*7. At the same time at the high Mach secondary design point the three-point optimization achieved as expected a higher drag reduction: C_D=304.0 counts (*Case_GBJ_*6) vs. C_D=295.0 counts (*Case_GBJ_*7) (compared with the original 321.5 counts). The resulting pressure distribution for the optimal generic business-jet configuration (*Case_GBJ_*7) is depicted in Fig.9.

The influence of the multipoint design on the optimized shapes vs. one-point optimization may be assessed from Fig.10. It can be observed that the requirements coming from the take-off design point, resulted in a significant reshape of the outboard wing and in a moderate change in the form of the leading and trailing edges, close to the crank section.

The comparison of the corresponding drag polars at the design Mach value is given in Fig. 11. The observed advantage of the three-point optimization, starting from $C_L = 0.4$, which increases at higher lift values, arises from the influence of the high Mach secondary design point.

Next let us present the results of comparison between two- and three-point optimizations (*Case_GBJ_*6 vs. *Case_GBJ_*7). In terms of shape, the influence of the third design point at a higher than cruise Mach value, mainly resulted in a moderate reshape of the wing tip airfoil.

In terms of lift/drag polars (see Fig.12 - 13), a slight advantage of *Case_GBJ_*7 noted at the main design Mach free-stream value, essentially increases at $M = 0.82$.

Another practically important off-design characteristics is Mach drag rise at fixed lift coefficient. The corresponding data may be found in Fig.14, where Mach drag rise curves at $C_L = 0.4$ for a one-point (*Case_GBJ_*2) and the three-point (*Case_GBJ_*7) optimizations are presented. In both cases, the optimization succeeded to shift the Mach drag divergence point to at least the main Mach design value, especially in the multipoint optimization. Specifically, based on the definition of Mach drag divergence point as the

Mach value in which $\partial C_D/\partial M = 0.1$, the corresponding M_{DD} value for the original configuration is equal to 0.795, while for the three-point optimization $M_{DD} = 0.815$. Additionally, the subsonic drag level (apparently due to reduction of form drag) is also decreased.

As it was mentioned in the problem statement, an additional off-design requirement is to preserve C_L^{max} value at the take-off conditions. It may be seen from Fig.15, that one-point optimizations do not necessarily support this property, while the multipoint optimizations in which the corresponding design point is included, allow to keep C_L^{max} to the required original level.

Finally, we present the results of a wing-body-fairing optimization. The corresponding optimal shapes are designated by *Case_GBJFR_*1 to *Case_GBJFR_*2.

The test case *Case_GBJFR_*1 deals with fairing optimization (with frozen exposed wing) without constraint on pitching moment and without beam constraints. The initial geometry for this optimization came from *Case_GBJ_*2. The second test case (*Case_GBJFR_*2) deals with wing optimization with the frozen wing-body fairing resulted from the *Case_GBJFR_*1 optimization.

As it was mentioned above the one-point wing optimization with the frozen fillet surface (labeled as *Case_GBJ_*2) achieved 16.7 counts of drag reduction. From the corresponding pressure distributions it was concluded that the achieved drag reduction may be attributed to a significant decrease in the shock strength in the exposed wing region.

At the same time, this optimization did not practically diminish the shock intensity at the wing-body-fairing region (see Fig.16). This conclusion may be drawn from the comparison between the corresponding chordwise pressure distributions at the spanwise coordinate $2y/b = 0.135$ located in the middle of the fairing region (see Fig.17).

The optimization of the wing-body-fairing shape (*Case_GBJFR_*1) improved the pressure distribution in the fillet region. As it can be seen from Fig.18 - 19, this optimization essentially diminished the shock strength in the fairing-wing junction while preserving an acceptable flow pattern on the exposed wing. As a result, this improvement permits to reduce the total drag of the optimized configuration by an additional 10.7 counts (compare to *Case_GBJ_*2) and to achieve the level $C_D = 264.6$ counts.

The shape achieved by the fillet optimization (*Case_GBJFR_*1) is shown in Fig.20 where non-dimensional sectional cuts of the optimal fairing are depicted.

We see, that optimal sectional shapes of the fillet tend to develop a convex-concave form on the upper surface which is further enhanced in the outboard direction. Note that frequently, in the aerodynamic practice, the upper surface of the wing root profile has a convex-concave form. Here, the optimizer discovered this trend automatically. Additionally, the trailing edge cusp nonexisting near the fuselage becomes significant at the sections close to the exposed wing.

The second test case *Case_GBJFR_*2, starting from *Case_GBJFR_*1 as an initial geometry, deals with the optimization of the exposed wing keeping the fairing shape frozen.

Data illustrating the results achieved in the framework of this optimization are given in Fig. 21 - 23. We see that the strength of the shock in the flow over the optimized business jet (*Case_GBJFR_*2) has significantly decreased.

The optimization *Case_GBJFR_*2 further improved the aerodynamic performance of the aircraft configuration: the total drag value is equal to 258.7 drag counts (5.9 counts less than that of the starting geometry *Case_GBJFR_*1).

Off-design behaviour of the optimized configurations may be studied through lift/drag polars. These are presented in Fig. 24, where the corresponding curves at $M = 0.80$ are compared with the original polars. It can be concluded that the local gains described above are preserved in a wide range of lift coefficient values from $C_L = 0.15$ to above $C_L = 0.6$. Additionally we should note that the drag reduction due to optimization increased for Mach numbers higher than the design value. Specifically, at $M = 0.82$ and $C_L = 0.40$ the drag reduction of

Case_GBJFR_2 with respect to the original business jet configuration, is equal to 42 counts.

5 Conclusions

The multiconstrained optimization of a generic business-jet aircraft has been considered. It may be concluded that the multipoint optimization allows for design of feasible aerodynamic shapes which possess a low drag at cruise conditions, satisfy a large number of geometrical and aerodynamic constraints and offer good off-design performance in markedly different flight conditions such as take-off conditions and high Mach zone.

5.1 Copyright Statement

References

[1] Jameson, A., Martinelli, L., and Vassberg, J., *Using computational fluid dynamics for aerodynamics - a critical cssessment*, Proceedings of ICAS 2002, Paper ICAS 2002-1.10.1, Optimage Ltd., Edinburgh, Scotland, U.K., 2002.

[2] Hicks, R. M., Henne, P. A., *Wing design by numerical optimization*, Journal of Aircraft, Vol. 15, No.4, 1978, pp.407-412.

[3] Jameson, A., *Aerodynamic design via control theory*, Journal of Scientific Computing, Vol. 3, No.2, 1988, pp.233-260.

[4] *Optimum Design Methods for Aerodynamics*, AGARD 1994; R-803.

[5] Vicini, A. and Quagliarella, D., *Inverse and direct airfoil design using a multiobjective genetic algorithm*, AIAA Journal, Vol. 35, No. 9, 1997, pp.1499–1505.

[6] Obayashi, S., Yamaguchi, Y. and Nakamura, T., *Multiobjective genetic algorithm for multidisciplinary design of transonic wing planform*, Journal of Aircraft, Vol. 34, No. 5, 1997, pp.690–693.

[7] Hajela, P., *Nongradient methods in multidisciplinary design optimization - status and potential*, Journal of Aircraft, Vol. 36, No. 1, 1999, pp.255-265.

[8] Mohammadi, B., and Pironneau, O., *Applied Shape Optimization for Fluids*, Oxford, Oxford University Press, 2001.

[9] Vassberg, J.C., and Gregg, R.D., *Overview of aerodynamic design for transport aircraft*, Proceedings of First M.I.T. Conference on Computational Fluid and Solid Mechanics, Cambridge, MA, MIT Press, June 2001.

[10] Epstein, B., and Peigin, S., *Constrained aerodynamic optimization of 3D wings driven by Navier-Stokes computations*, AIAA Journal, Vol. 43, No. 9, 2005, pp.1946-1957.

[11] Epstein, B., Rubin, T., and Seror, S., *Accurate multiblock Navier-Stokes solver for complex aerodynamic configurations*, AIAA Journal, Vol. 41, No. 4, 2003, pp.582–594.

[12] Seror, S., Rubin, T., Peigin, S. and Epstein, B., *Implementation and validation of the Spalart-Allmaras turbulence model for a parallel CFD code*, Journal of Aircraft, Vol. 42, No.1, 2005, pp.179–188.

[13] Epstein, B., and Peigin, S., *Robust hybrid approach to multiobjective constrained optimization in eerodynamics*, AIAA Journal, Vol. 42, No.8, 2004, pp.1572–1581.

[14] Michalewicz, Z., *Genetic Algorithms + Data Structures = Evolution Programs*, New-York: Springer Verlag, 1996.

[15] Peigin, S., Epstein, B., Rubin, T., and Seror, S., *Parallel large scale high accuracy Navier-Stokes computations on distributed memory clusters*, The Journal of Supercomputing, Vol. 27, 2004, pp.49–68.

[16] Epstein, B., Averbuch, A., and Yavneh, I., *An accurate ENO driven multigrid method applied to 3D turbulent transonic flows*, Journal of Computational Physics, Vol.168, 2001, pp.316–338.

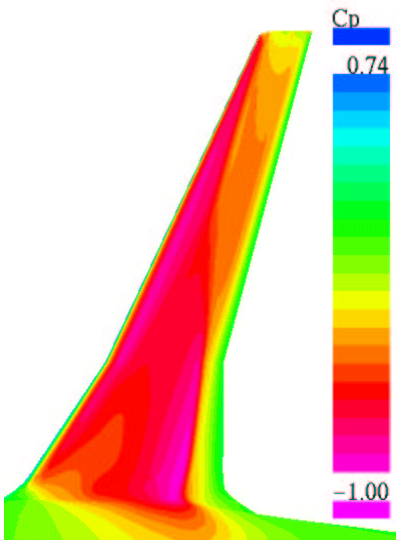

Fig. 1 Original generic business jet wing-body. Pressure distribution on the upper surface of the wing at $M = 0.80$, $C_L = 0.40$.

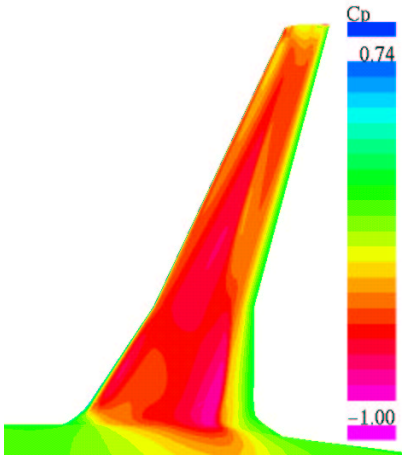

Fig. 3 Optimized generic business jet wing-body - *Case_GBJ_2*. Pressure distribution on the upper surface of the wing at $M = 0.80$, $C_L = 0.40$.

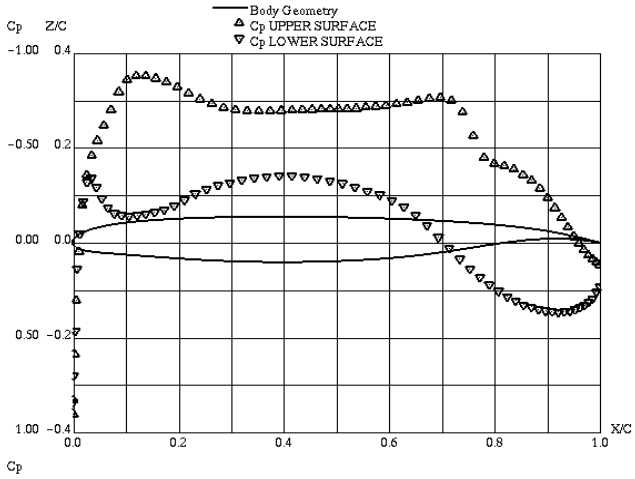

Fig. 2 Original generic business jet wing-body. $M = 0.80$, $C_L = 0.40$. Chordwise pressure distribution at $2y/b = 0.44$.

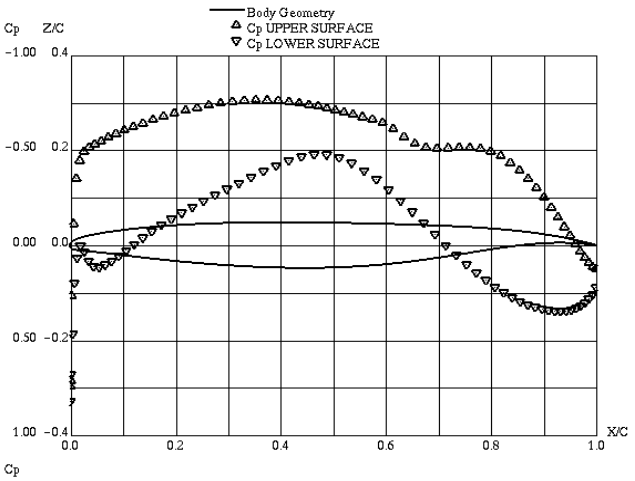

Fig. 4 Optimized generic business jet wing-body - *Case_GBJ_2*. $M = 0.80$, $C_L = 0.40$. Chordwise pressure distribution at $2y/b = 0.44$.

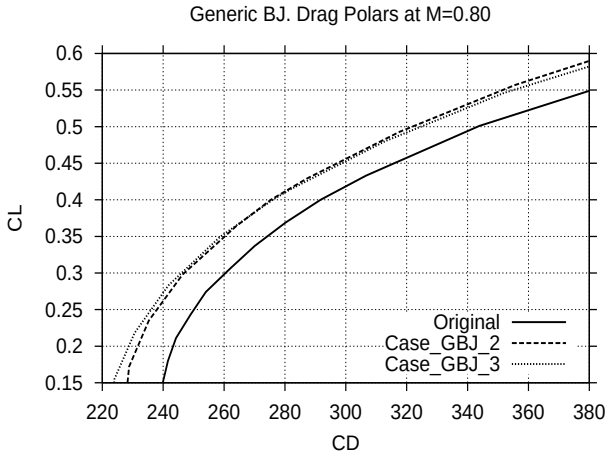

Fig. 5 Generic business jet wing-body. Drag polars at M=0.80. Optimized configurations vs. the original one.

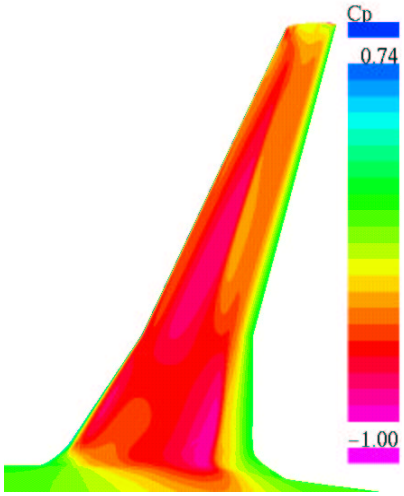

Fig. 7 Optimized generic business jet wing-body - *Case_GBJ_*5. Pressure distribution on the upper surface of the wing at $M = 0.80, C_L = 0.40$.

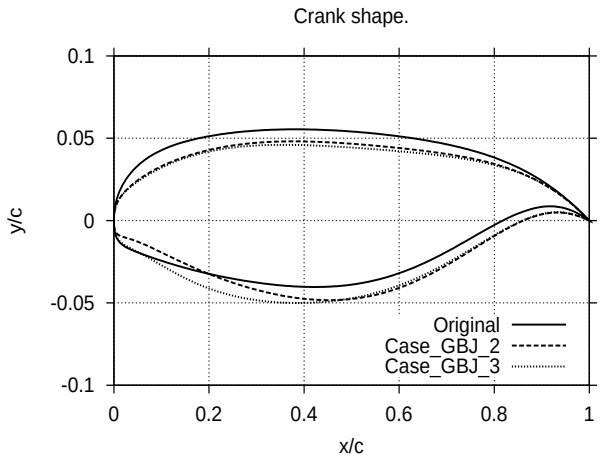

Fig. 6 Optimization of the generic business jet. Crank section: *Case_GBJ_*2 and *Case_GBJ_*3 vs. initial geometry.

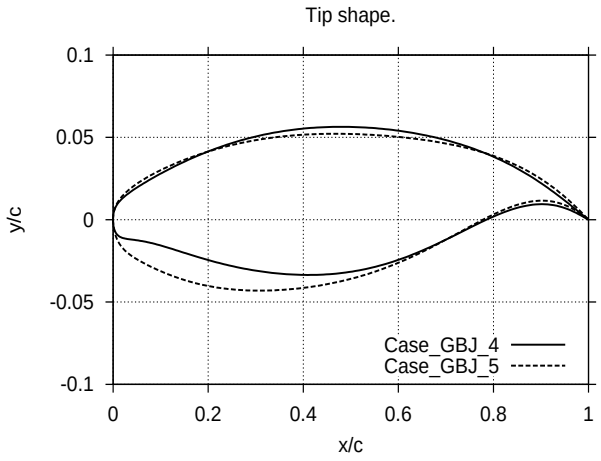

Fig. 8 Optimization of the generic business jet. Tip section: *Case_GBJ_*4 vs. *Case_GBJ_*5.

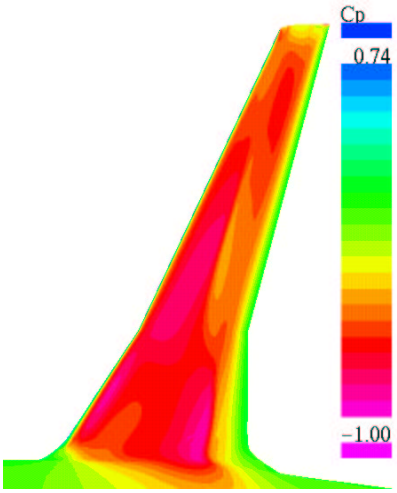

Fig. 9 Optimized generic business jet wing-body - *Case_GBJ_7*. Pressure distribution on the upper surface of the wing at $M = 0.80, C_L = 0.40$.

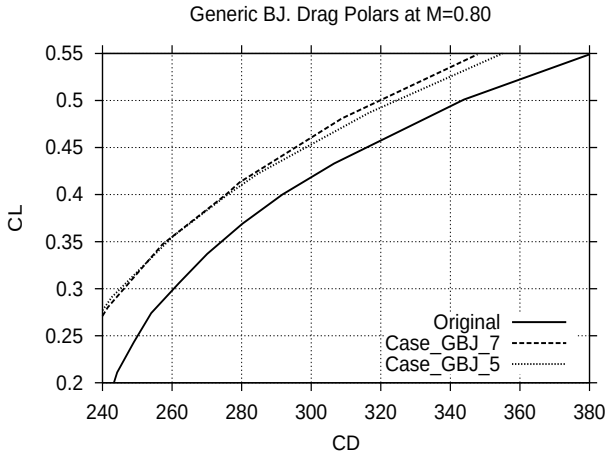

Fig. 11 Generic business jet wing-body. Drag polars at M=0.80. Optimized configurations vs. the original one.

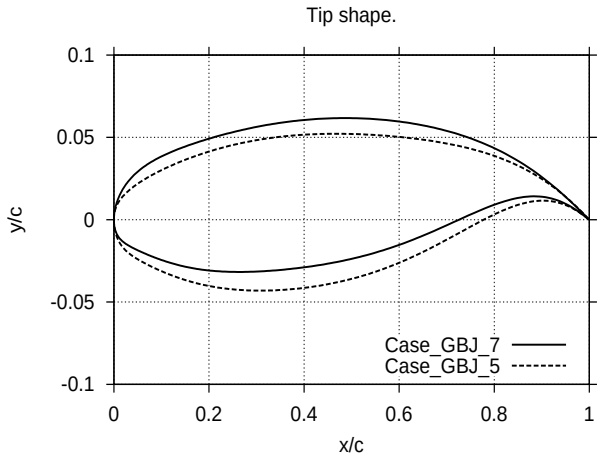

Fig. 10 Optimization of the generic business jet. Tip section: *Case_GBJ_5* vs. *Case_GBJ_7*.

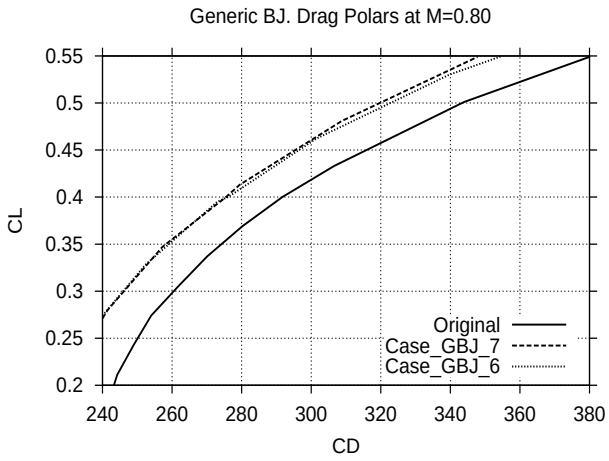

Fig. 12 Generic business jet wing-body. Drag polars at M=0.80. Optimized configurations vs. the original one.

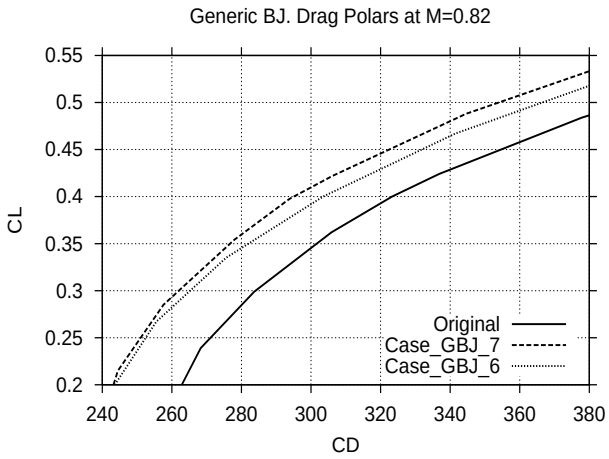

Fig. 13 Generic business jet wing-body. Drag polars at M=0.82. Optimized configurations vs. the original one.

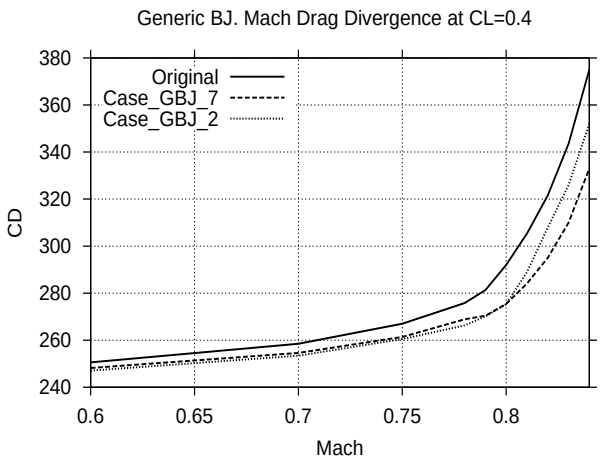

Fig. 14 Generic business jet wing-body. Mach drag divergence at $C_L = 0.40$. Optimized configurations vs. the original one.

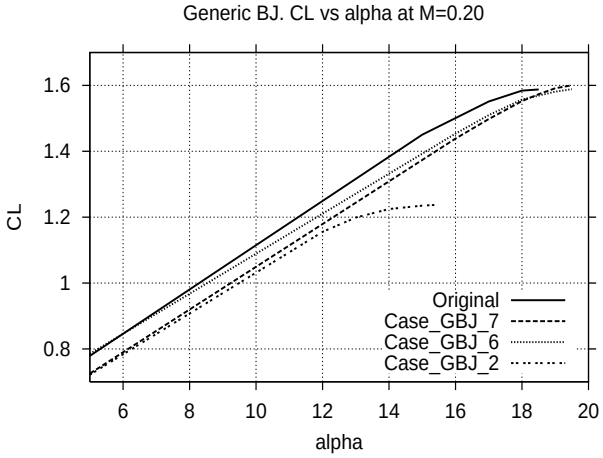

Fig. 15 Generic business jet wing-body. Lift vs. angle of attack curves at $M = 0.20$. Optimized configurations vs. the original one.

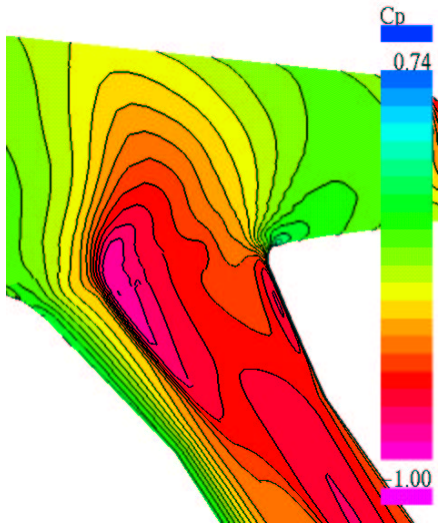

Fig. 16 Generic business jet. Pressure distribution at the wing-body-fairing region for $M = 0.80$, $C_L = 0.4$. Optimized configuration *Case_GBJ_2*.

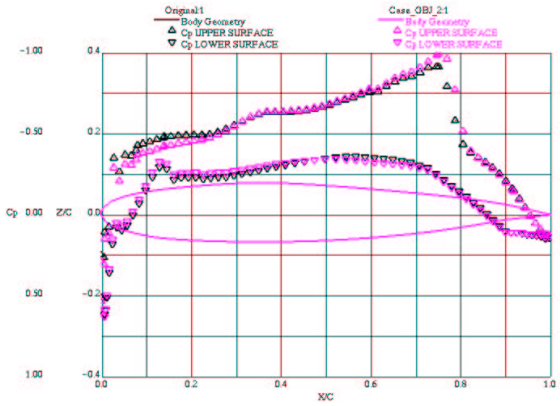

Fig. 17 Generic business jet. Original configuration vs. *Case_GBJ_2*. Chordwise pressure distribution for $M = 0.80$, $C_L = 0.4$ at $2y/b = 0.135$.

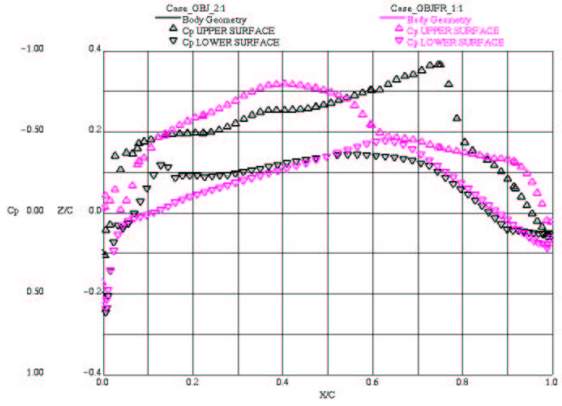

Fig. 19 Generic business jet. Optimized configuration *Case_GBJFR_1* vs. *Case_GBJ_2*. Chordwise pressure distribution for $M = 0.80$, $C_L = 0.4$ at $2y/b = 0.135$.

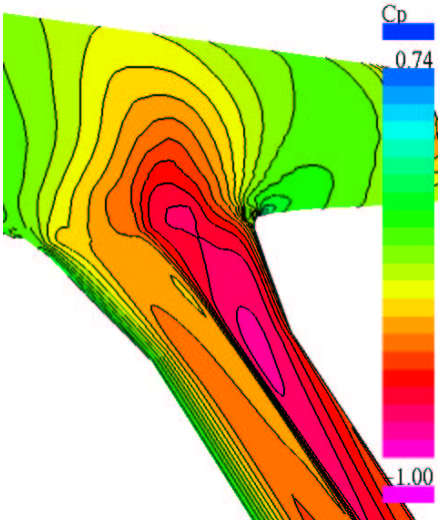

Fig. 18 Generic business jet. Pressure distribution at the wing-body-fairing region for $M = 0.80$, $C_L = 0.4$. Optimized configuration *Case_GBJFR_1*.

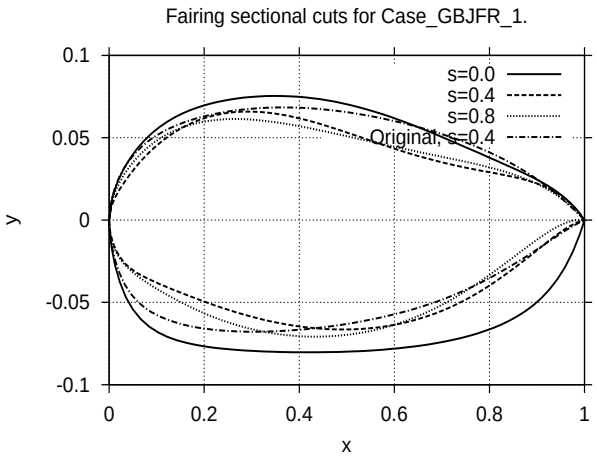

Fig. 20 Generic business jet. Shape of sectional cuts at the fairing region. Optimized configuration *Case_GBJFR_1*.

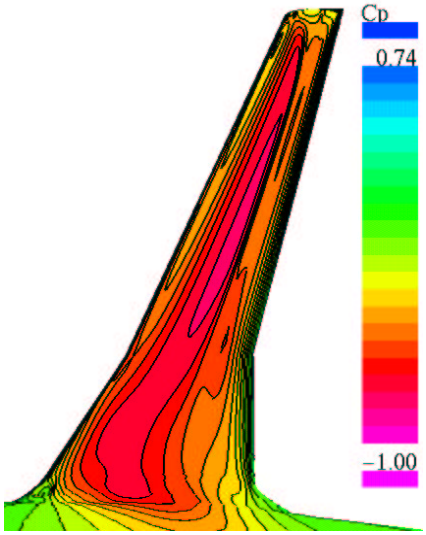

Fig. 21 Generic business jet. Pressure distribution on the wing upper surface for $M = 0.80$, $C_L = 0.4$. Optimized configuration *Case_GBJFR_2*.

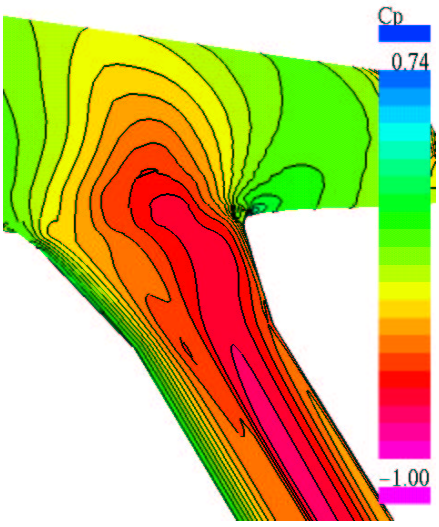

Fig. 22 Generic business jet. Pressure distribution at the wing-body-fairing region for $M = 0.80$, $C_L = 0.4$. Optimized configuration *Case_GBJFR_2*.

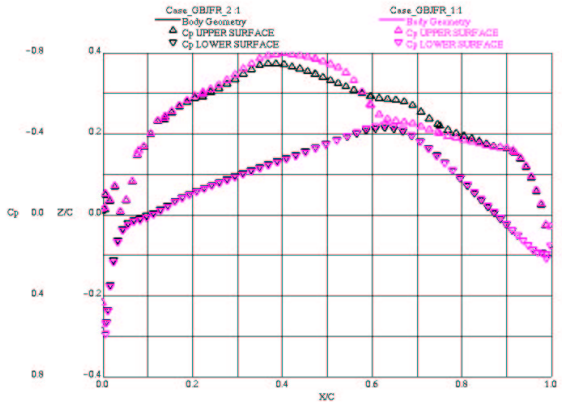

Fig. 23 Generic business jet. Optimized configuration *Case_GBJFR_1* vs. *Case_GBJFR_2*. Chordwise pressure distribution for $M = 0.80$, $C_L = 0.4$ at $2y/b = 0.135$.

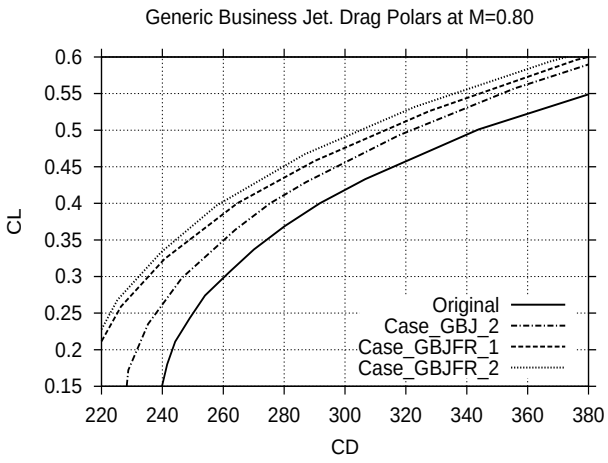

Fig. 24 Generic business jet. Drag polars at $M = 0.80$. Original configuration vs. optimized ones.